# Resistance Modeling for Striplines with Different Surface Roughness on the Planes

Shaohui Yong<sup>#1</sup>, Victor Khilkevich<sup>#2</sup>, Yuanzhuo Liu<sup>#3</sup>, Jiayi He<sup>#4</sup>, Han Gao<sup>+5</sup>, Scott Hinaga<sup>+6</sup>, Darja Padilla<sup>+7</sup>,
Douglas Yanagawa<sup>+8</sup>, Jun Fan<sup>#9</sup>, James Drewniak<sup>#10</sup>,

\*EMC Laboratory, Missouri University of Science and Technology, Rolla, MO. 65401 USA

\*Cisco Systems, Inc, San Jose, CA. 95134 USA

<sup>1</sup>sy2m5, <sup>2</sup>khilkevichv, <sup>3</sup>liuyuanz, <sup>4</sup>hejiay, <sup>9</sup>jfan, <sup>10</sup>drewniak@mst.edu

<sup>5</sup>hgao2, <sup>6</sup>shinaga, <sup>7</sup>darja, <sup>8</sup>yanagawa@cisco.com

Abstract-To model additional conductor loss due to foil surface roughness various empirical or physical models have been brought up to provide surface roughness correction factors for the per-unit-length (PUL) resistance assuming certain roughness of foil conductors. However for striplines on typical printed circuit board, different sides of the traces and references planes may have different surface roughness levels due to the fabrication process. Traditionally engineers may calculate surface roughness correction factors using averaged roughness level of the upper and lower sides of the trace. However this empirical estimation may lead to inaccurate modeling results especially when the stripline is not vertically symmetrical or the differences among the roughness levels of planes are significant. In this project, a methodology is presented to calculate the resistance of a stripline with different surface roughness levels on upper and lower sides of the trace and reference planes. After separating the resistances contributed by different smooth planes, each plane's resistance is corrected independently using corresponding surface roughness correction factor. The stripline's resistance is obtained by combining the corrected resistances of different planes.

Index Terms—Skin effect, surface roughness, striplines, printed circuit boards, signal integrity

## I. INTRODUCTION

Conductor loss is an increasingly important factor affecting the signal integrity (SI) performance for high-speed channels. It has been quite evident that the skin-effect formulas ignoring foil surface roughness underestimate attenuation as frequency goes up to tens of gigahertz [1-3]. Various approaches [4-9] have been proposed to calculate the frequency-dependent surface roughness correction factor using the cross-sectional profile or the root-mean-square (RMS) roughness levels.

However, the previously proposed surface roughness modeling approaches assumed equal roughness on all conductor surfaces instead of modelling realistic stripline structures consisting of four rough planes (the upper and lower sides of the traces, and the upper and lower reference planes). Actually, different surface roughness levels on different planes can be commonly observed due to printed circuit boards (PCB) fabrication process. To provide better adhesion between copper and epoxy resin, various foil treatments are applied by PCB vendors to roughen up certain sides of the planes [10-13]. In addition, the electrodeposition (ED) process leads to foil with

one side smoother and the other side rougher [6][13]. As the SEM image shows in Fig. 1, the upper and lower sides of the trace, as well as the upper and lower reference planes have noticeable difference in terms of surface roughness levels. Traditionally SI engineers may use the averaged surface roughness levels of all planes to calculate the surface roughness correction factor, assuming different planes have similar contribution to the total resistance. However, as section II will show, the averaging approach leads to results with low accuracy. A more precise modeling approach is needed.

The authors will start from the analysis of the PUL resistance contributions of different smooth planes. The surface roughness correction factors determined by approaches presented in [4-9] are applied to the smooth planes' resistances accordingly. The rough single-ended or coupled stripline resistance is calculated by combining the corrected resistances of each rough plane.

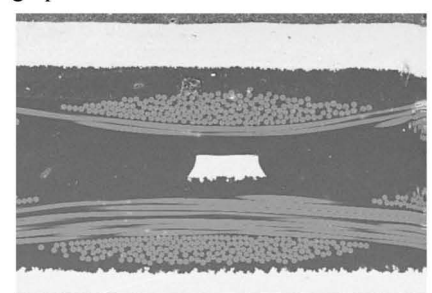


Fig.1. The SEM image of a stripline. It can be observed that different planes (upper and lower sides of the trace and the referene) on stripline have different surface roughness.

## II. SINGLE-ENDED STRIPLINES

#### A. Conductor loss of striplines

Let us start from some basics about stripline conductor loss. The upper and lower ground planes of the stirpline have the same potential, and the signal line has different potential. The cross-section of the stripline is illustrated in Fig.2(a). As frequency goes up the AC resistance due to skin effect will cause the current distribution concentrated on the edges. In a vertically asymmetrical stripline  $(h_1 \neq h_2)$ , the resistances of the upper  $(R_{h1})$  and lower edges  $(R_{h2})$  of the line will differ due to unbalanced cross-sectional area where the current is flowing. According to [14, (5-18)],  $R_{h1}$  and  $R_{h2}$  are modeled using the resistances of the trace  $(R_{t1}, R_{t2})$  and reference plane  $(R_{r1}, R_{r2})$ 

in series:

$$R_{h1} = R_{t1} + R_{r1} R_{h2} = R_{t2} + R_{r2}$$
 (1)

According to [14, (5-19)], the total resistance of a stripline is modeled by the resistances of the upper and lower portions  $(R_{h1}, R_{h2})$  in parallel. The total resistance of the single-ended stripline with smooth surfaces is expressed therefore as:

$$R_{se} = \frac{R_{h1} \cdot R_{h2}}{R_{h1} + R_{h2}} = \frac{(R_{t1} + R_{r1}) \cdot (R_{t2} + R_{r2})}{R_{t1} + R_{r1} + R_{t2} + R_{r2}}$$
(2)

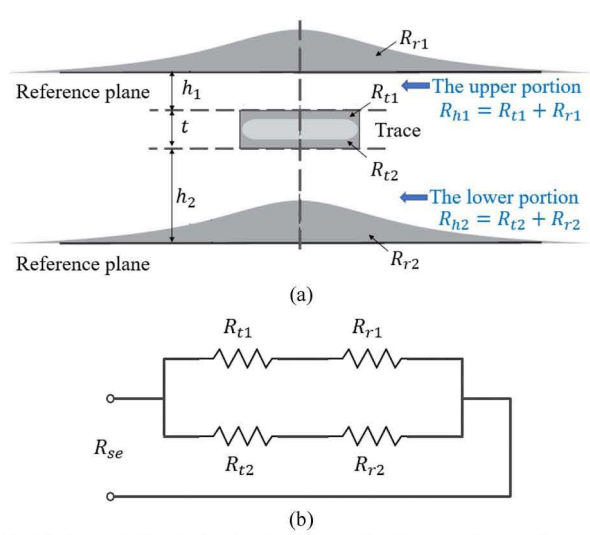


Fig.2. (a) Current distribution in the trace and reference planes of a smooth stripline [14, Figure 5-8]. The resistance of the upper and lower side of the trace, as well as the upper and lower reference planes are expressed as  $R_{t1}$ ,  $R_{t2}$ ,  $R_{r1}$   $R_{r2}$  respectively. (b) The equivlent resistance circuit for a single-ended stripline.

Compared to the case with smooth foil surfaces, additional conductor loss due to absorption and scattering is introduced when rough foil surfaces are taken into account [7]. The resistance increment is usually modeled using a frequency-dependent correction factor [4-9]. Different planes with different roughness levels can be modeled by four independent surface roughness correction factors  $(K_{t1}, K_{t2}, K_{r1}, K_{r2}$  illustrated in Fig. 3).

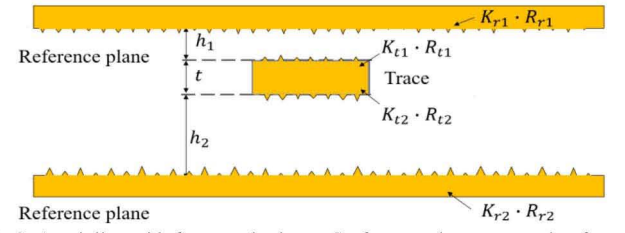


Fig.3. A stripline with four rough planes. Surfcae roughness correction factors for the upper side of the trace  $(K_{t1})$ , lower side of the trace  $(K_{t2})$ , upper reference plane  $(K_{r1})$ , lower reference plane  $(K_{r2})$  are used to model the resistance of corresponding rough planes.

The resistances contributed by the top and bottom portions of the stripline with rough foil surfaces are expressed as:

$$R_{h1,SR} = K_{t1} \cdot R_{t1} + K_{r1} \cdot R_{r1} R_{h2,SR} = K_{t2} \cdot R_{t2} + K_{r2} \cdot R_{r2}$$
(3)

According to (2), the expression of the total resistance of the single-ended stripline with four rough planes is:

$$R_{se,SR} = \frac{R_{h1,SR} \cdot R_{h2,SR}}{R_{h1,SR} + R_{h2,SR}}$$

$$= \frac{(K_{t1}R_{t1} + K_{r1}R_{r1})(K_{t2}R_{t2} + K_{r2}R_{r2})}{K_{t1}R_{t1} + K_{r1}R_{r1} + K_{t2}R_{t2} + K_{r2}R_{r2}}$$
(4)

Thus, if the resistance contributed by different smooth planes  $(R_{t1}, R_{t2}, R_{r1}, R_{r2})$  can be calculated, the rough stripline can be modeled using (4) with known surface roughness correction factors  $(K_{t1}, K_{t2}, K_{r1}, K_{r2})$ . However, a 2D or 3D solver only provides the total PUL resistance of the stripline (not the plane contributions). In the following subsection, an approach to calculate the resistances of four smooth planes  $(R_{t1}, R_{t2}, R_{r1}, R_{r2})$  will be presented.

## B. Resistances contributed by different planes

Since the distances between the reference planes and the trace  $(h_1 \text{ and } h_2)$  are the determinant factors for the resistance [14], two additional 2D models with vertically symmetrical geometry are created to calculate the upper and lower portions' resistance  $(R_{h1}, R_{h2})$  of the stripline. As Fig. 4 illustrates, the current distribution in the upper and lower portions of these models are supposed to be the same due to the symmetry.

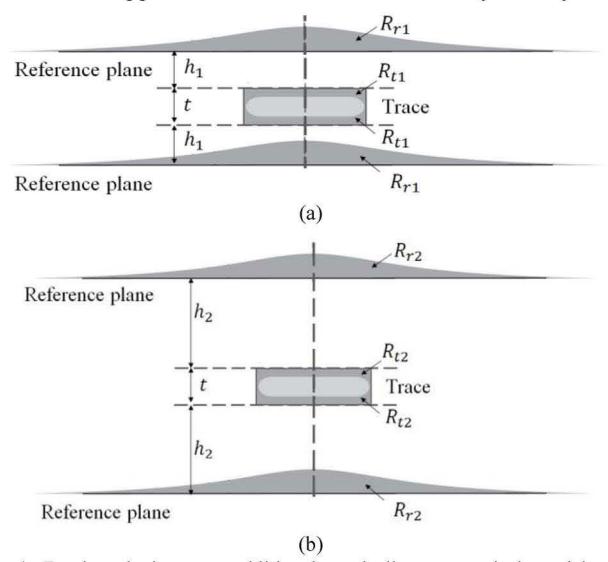


Fig.4. By introducing two additional vertically symmetrical models, the resistances of the upper portion of the striplines  $(R_{h1})$  and lower portion of the striplines  $(R_{h2})$  are calculated using the resistances  $(R_{sy,h1}, R_{sy,h2})$  of the 2D models illustrated by (a) and (b).

The resistances contributed by the upper  $(R_{sy,h1})$  and lower  $(R_{sy,h2})$  portions are calculated in models (a) and (b). According to (2), the upper and lower portions are in parallel. Thus, the resistances of the upper and lower portions of the stripline are calculated as:

$$R_{h1} = 2R_{sy,h1} R_{h2} = 2R_{sy,h2}$$
 (5)

By inserting (5) into (2), the total resistance of the stripline can be modeled as:

$$R_{se} = \frac{2 \cdot R_{sy,h1} \cdot R_{sy,h1}}{R_{sy,h1} + R_{sy,h2}} \quad (6)$$

To verify the modeling approach presented by (6), a single-ended stripline model with cross-sectional geometry

shown in Fig. 5 is created using Ansys Q2D [15]. The total resistance of the stripline  $(R_{se})$  is calculated directly by the 2D simulation for reference. Two additional 2D models with symmetrical geometry (illustrated by Fig.6) are created to calculate the resistances of the stripline's upper and lower portion  $(R_{sv,h1})$  and  $R_{sv,h2}$ .

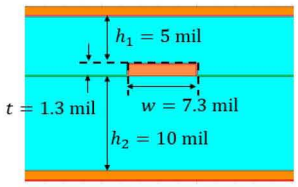


Fig. 5 The cross-sectional geometry of the single-ended stripline.

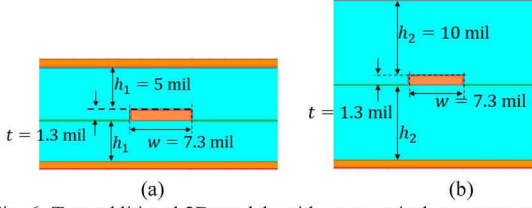


Fig. 6. Two additional 2D models with symmetrical geometry are introduced. Model (a) and (b) are vertically balanced with trace to reference distance equal to  $h_1$  and  $h_2$ .

The comparison between directly simulated  $R_{se}$  and modeled  $R_{se}$  using (6) is performed. According to Fig. 7 (b), the modeled  $R_{se}$  has a very good match (below 3% difference) with the directly simulated  $R_{se}$ .

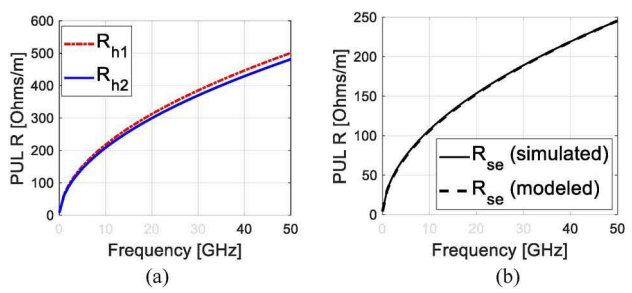


Fig. 7. (a):  $R_{h1}$  and  $R_{h2}$  calculated using the additional 2D models illustrated by Fig. 6; (b): comparison between  $R_{se}$  simulated directly by the 2D model and  $R_{se}$  modeled using  $R_{h1}$  and  $R_{h2}$ .

In addition to calculating the resistances of the upper and lower portions of the stripline, the contribution from the reference plane and the trace can be further separated by assigning a perfect electric conductor (PEC) to the trace or reference plane. For example, to calculate the resistance of the upper side of the trace ( $R_{t1}$ ) for the stripline illustrated in Fig.5, the 2D model illustrated by Fig. 8 (a) is created. By assigning PEC to the reference planes, the resistance of reference plane is excluded.  $R_{sy,h1}^{PEC,R}$  is calculated by the 2D model, and it is equal to the resistance of the two symmetrical 'upper sides' of the trace in parallel. Thus, the resistances of different planes are calculated:

$$R_{t1} = 2R_{sy,h1}^{PEC,R}$$

$$R_{r1} = 2R_{sy,h1}^{PEC,T}$$

$$R_{t2} = 2R_{sy,h2}^{PEC,R}$$

$$R_{r2} = 2R_{sy,h2}^{PEC,T}$$
(7)

where,  $R_{sy,h1}^{PEC,R}$ ,  $R_{sy,h1}^{PEC,T}$ ,  $R_{sy,h2}^{PEC,R}$  and  $R_{sy,h2}^{PEC,T}$  are calculated by the 2D models illustrated by Fig.8 (a-d) respectively.

By inserting (7) into (2), the resistance of the stripline can be modeled as:

$$R_{se} = \frac{2 \cdot (R_{sy,h1}^{PEC,R} + R_{sy,h1}^{PEC,T}) \cdot (R_{sy,h2}^{PEC,R} + R_{sy,h2}^{PEC,T})}{R_{sy,h1}^{PEC,R} + R_{sy,h1}^{PEC,T} + R_{sy,h2}^{PEC,R} + R_{sy,h2}^{PEC,T}}$$
(8)

To validate the modeling approach expressed by (8), using the stripline geometry in Fig.5, the resistances of four different planes are calcaulted using the additional models illustrated by Fig. 8. The modeled  $R_{se}$  calculated by (8) has a good mach with simulated  $R_{se}$  as Fig. 9(b) shown.

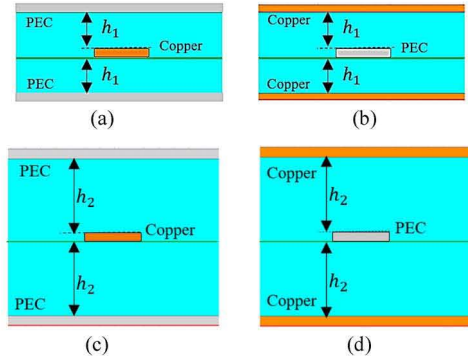


Fig.8. Four additional 2D models are introducted to calculate resistances of the upper side of the trace  $R_{t1}$  (a), upper reference plane  $R_{r1}$  (b), lower side of the trace  $R_{t2}$  (c), and lower reference plane  $R_{r2}$  (d).

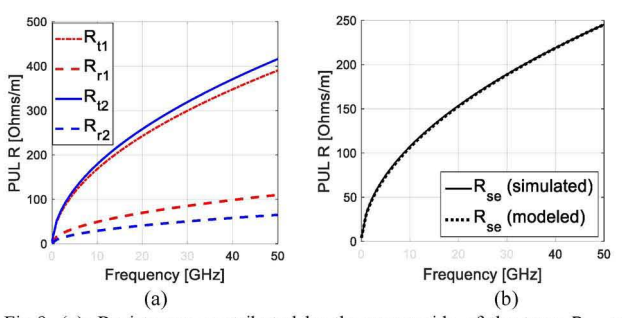


Fig.9. (a): Resistances contributed by the upper side of the trace  $R_{t1}$ , upper reference plane  $R_{r1}$ , lower side of the trace  $R_{t2}$ , and lower reference plane  $R_{r2}$ ; (b): comparision between  $R_{se}$  calculated by the 2D solver and  $R_{se}$  modeled using (8).

#### C. Striplines with different roughness levels on the planes

After calculating the resistances of four smooth planes  $(R_{t1}, R_{t2}, R_{r1}, R_{r2})$ , four independent surface roughness corrections factors can be easily taken into account. By inserting (7) into (4), the resistance of the stripline can be modeled as:

$$R_{se,SR} = \frac{2(K_{t1}R_{sy,h1}^{PEC,R} + K_{r1}R_{sy,h1}^{PEC,T})(K_{t2}R_{sy,h2}^{PEC,R} + K_{r2}R_{sy,h2}^{PEC,T})}{K_{t1}R_{sy,h1}^{PEC,R} + K_{r1}R_{sy,h1}^{PEC,T} + K_{t2}R_{sy,h2}^{PEC,R} + K_{r2}R_{sy,h2}^{PEC,T}}$$
(9)

To validate (9), using the stripline illustrated by Fig.5, three cases with rough surfaces are created using Ansys Q2D. The surface roughness is modeled using Hammerstad approach [4].

To calculate the modeled  $R_{se,SR}$ , the resistances contributed by different planes are determined by introducing four additional 2D models illustrated by Fig. 8. The surface roughness correction factors  $(K_{t1}, K_{r1}, K_{t2}, K_{r2})$  are calculated using the expression presented in Hammerstad's paper [4] (same model is used by the 2D solver). The comparison between the modeled  $R_{se,H}$  calculated using (9) and Q2D simulated  $R_{se,SR}$  is shown in Fig. 10. Good agreement can be achieved with the difference below 5%. The traditional modeling approach using averaged RMS roughness levels of four surfaces is presented for the third case. As can be seen, averaging roughness leads to poor agreement.

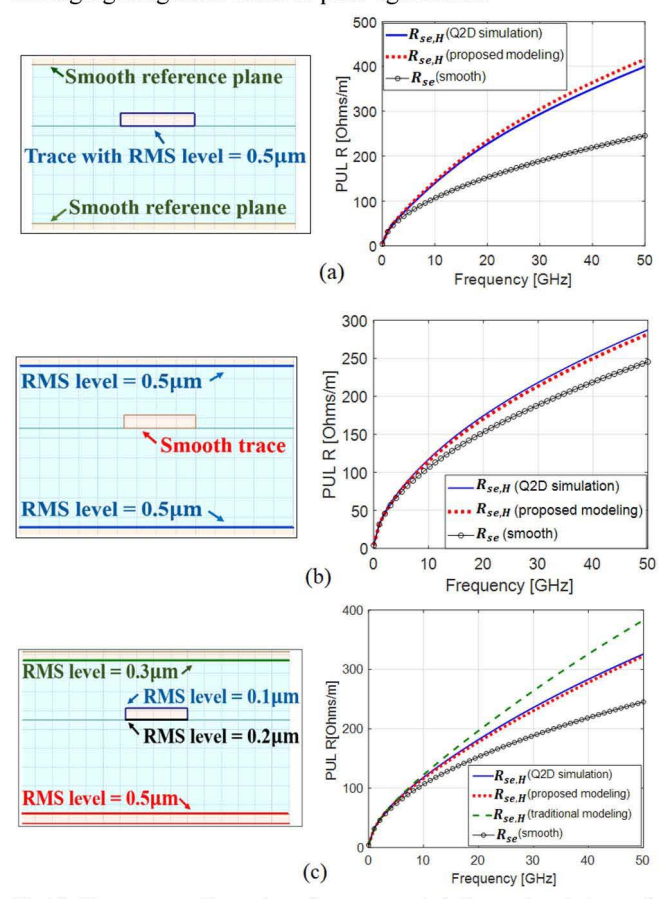


Fig.10. Three cases with rough surfaces are created. Comparison between the modeling and simulation is presented.

#### III. COUPLED STRIPLINES MODELING

To model the coupled stripline pair, the expressions for the single-ended stripline, (2) and (4) are extended for common and differential mode (derivation is given in the Appendix). The resistances of the stripline pair with smooth  $(R_m)$  and rough planes  $(R_{m,SR})$  are expressed as:

$$R_{m} = \frac{(R_{t1,m} + R_{r1,m}) \cdot (R_{t2,m} + R_{r2,m})}{R_{t1,m} + R_{r1,m} + R_{t2,m} + R_{r2,m}}$$
(10)  

$$R_{m,SR} = \frac{(K_{t1}R_{t1,m} + K_{r1}R_{r1,m}) \cdot (K_{t2}R_{t2,m} + K_{r2}R_{r2,m})}{K_{t1}R_{t1,m} + K_{r1}R_{r1,m} + K_{t2}R_{t2,m} + K_{r2}R_{r2,m}}$$
(11)

where, m represents the mode (common or differential). To calculate the resistances contributed by different planes, we use an idea similar to that in (7), i.e. the resistances of upper side of the trace  $(R_{t1,m})$ , upper reference plane  $(R_{r1,m})$ , lower side of the trace  $(R_{t2,m})$ , and lower reference plane  $(R_{r2,m})$  are calculated using additional models illustrated by Fig.11. Relationship between the surface contributions and the four model resistances are given (similar to the single-ended case)

by:

$$\begin{split} R_{t1,m} &= 2R_{sy,h1,m}^{PEC,R} \\ R_{r1,m} &= 2R_{sy,h1,m}^{PEC,T} \\ R_{t2,m} &= 2R_{sy,h2,m}^{PEC,R} \\ R_{r2,m} &= 2R_{sy,h2,m}^{PEC,T} \end{split} \tag{12}$$

To validate (10) the stripline pair illustrated by Fig.12 is used. The differential and common mode resistances of four planes ( $R_{t1,m}$ ,  $R_{r1,m}$ ,  $R_{t2,m}$ ,  $R_{r2,m}$ ) are calcaulted using four additional models illustrated by Fig. 11.

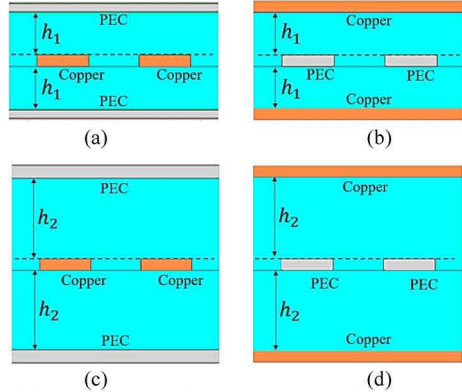


Fig.11. Four 2D models are introducted to extract resistance contributed by the upper side of the trace  $R_{t1,m}$  (a), upper reference plane  $R_{r1,m}$  (b), lower side of the trace  $R_{t2,m}$  (c), and lower reference plane  $R_{r2,m}$  (d).

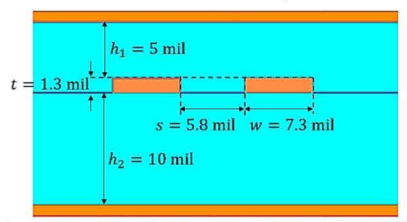


Fig.12. The cross-sectional geometry of the coupled stripline pair.

To validate the proposed rough surfaces modeling approach expressed by (11) on three coupled pair with different roughness on the surfaces illustrated by Fig. 13, three rough cases are created. The simulated  $R_{m,H}$  is calculated directly by Q2D, and modeled  $R_{m,H}$  is calculated using (11) with  $R_{t1,m}$ ,  $R_{r1,m}$ ,  $R_{t2,m}$ ,  $R_{r2,m}$  obtained from (12) and  $K_{t1}$ ,  $K_{r1}$ ,  $K_{t2}$ ,  $K_{r2}$  calculated by Hammerstad model's expression. As can be seen from Fig. 13 good agreement between the simulated and modelled resistances is achieved in all three cases.

The validation is also performed using CST 3D models [16] presented in Fig. 14 and 15. Since the dielectric substrate in the models is air, there is no dielectric loss. For practical low-loss transmission lines with  $R \ll \omega L$ , the attenuation factor can be calculated as:  $\alpha = 0.5R\sqrt{C/L}$  [17, (2.85a)]. Thus, the attenuation factors of the 3D models with lossless dielectric material are proportional to the resistances and the surface roughness correction factors can be used to correct the attenuation factor directly.

As Fig. 14 and 15 illustrate, the surface roughness is modelled using the hemispheres placed on the smooth planes. The surface roughness correction factor for the rough surface is

calculated using the ratio of the rough and smooth attenuation factors in the model in Fig. 14. Analytical surface roughness models are not used here to avoid additional inaccuracies due to approximated correction factor. For simulation of practical PCB traces, a certain roughness model will be needed.

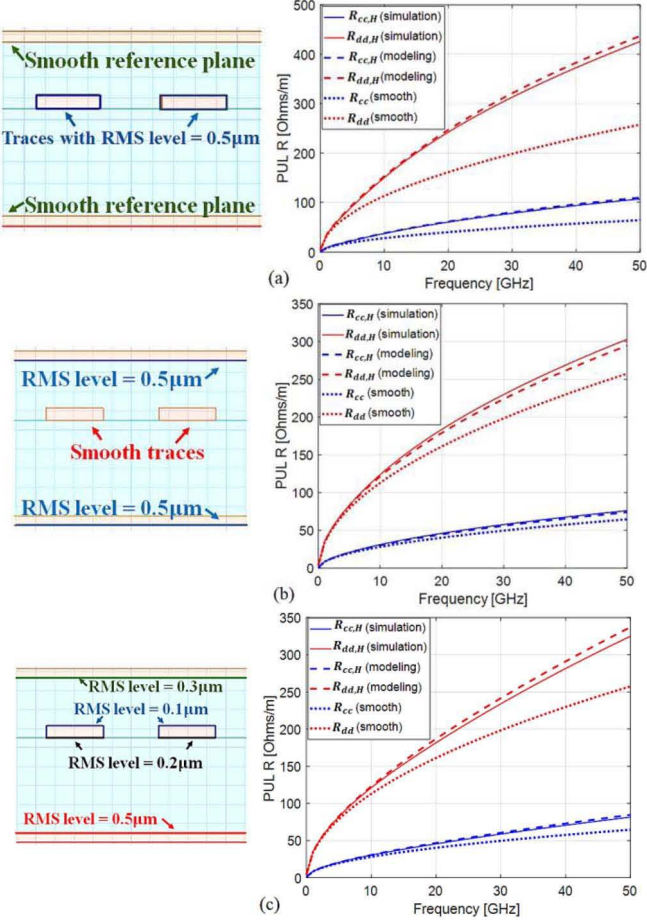


Fig.13. Three cases with rough surfaces are created. The compairiosn between the modeling and simulation is presented.

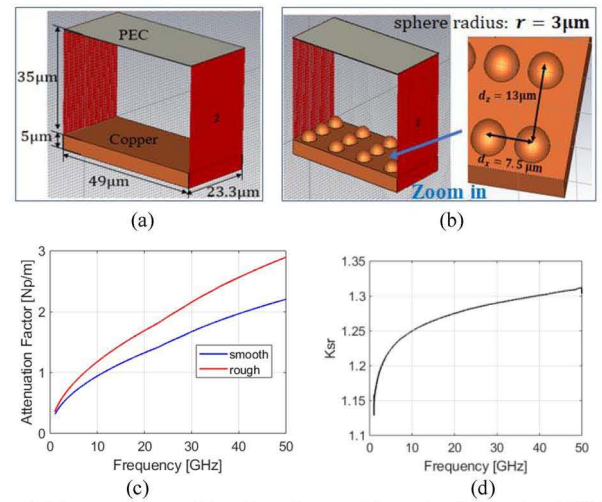


Fig.14. The smooth trace (a) and rough trace (b) are simulated using CST. The attenuation factors (c) are calcualted using the simulated insertion loss. The surface roughness correction factor (d) is the ratio of the rough and smooth attenuation factors.

Two cases with rough surfaces are simulated by CST. The

modeled  $\alpha_m$  is calculated using the proposed approach by introducing four additional models. As Fig. 15 shows, a good match is achieved between the simulation and the modeling results in two cases: smooth trace / rough reference planes, and rough trace / smooth reference planes.

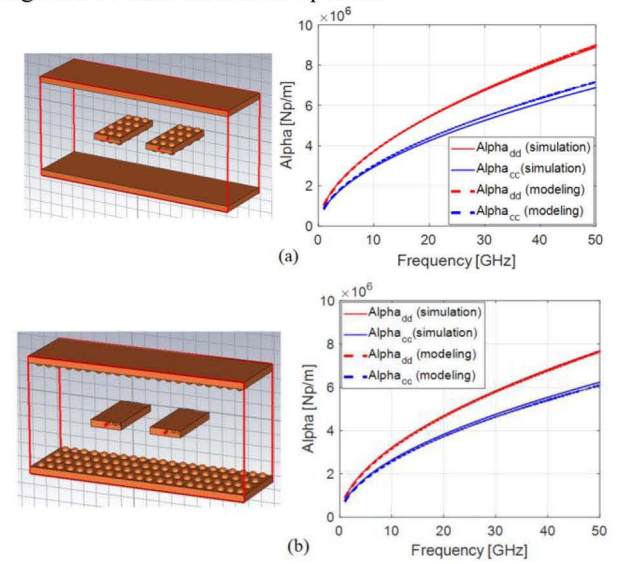


Fig.15. Two cases with rough surfaces are created. The compairiosn between the modeled and simulated  $\alpha_{cc}$  and  $\alpha_{dd}$  is presented.

#### IV. CONCLUSION

This paper provides a more comprehensive modeling for striplines with different surface roughness on different planes compared to the traditional roughness averaging approach. The resistances contributed by the planes are calculated using four additional stripline models, and corrected by independent surface roughness correction factors accordingly. According to 2D and 3D simulation results, the total modeled resistances for single-ended and coupled striplines provide much better accuracy compared to the models with averaged roughness.

#### V. APPENDIX

The derivation of (10) for common and differential mode is shown in this section. Let us take a closer look at the current distribution of a coupled stripline pair. As Fig.A-1 illustrates, the exclusive return path for the left or right trace is expressed as  $R_r$ , and the mutual return path is expressed as  $R_m$ .

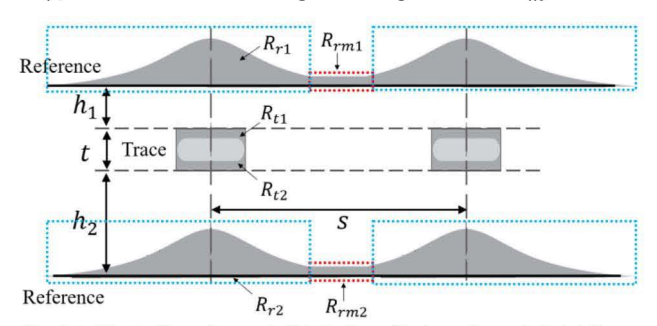


Fig.A-1. Illustration of current distribution of balanced coupled striplines.

When the separation between two traces (s) is infinite, there is no coupling between lines and  $R_m = 0$ . When the separation between two traces (s) is zero (a single ended line) no exclusive

return path exists and  $R_r = 0$ . The definition of PUL nodal resistance matrix (R) for balanced coupled lines is shown in (A1), and the matrix elements  $R_{11}$  and  $R_{21}$  are calculated by (A2) and (A3).

$$\begin{bmatrix} V_1 \\ V_2 \end{bmatrix} = R \cdot \begin{bmatrix} I_1 \\ I_2 \end{bmatrix} \text{, where } R = \begin{bmatrix} R_{11} & R_{21} \\ R_{21} & R_{11} \end{bmatrix} \text{ (A1)}$$

$$\text{when } V_2 = 0, \qquad R_{11} = \frac{V_1}{I_1} = R_t + R_r + R_{rm} \text{ (A2)}$$

$$\text{when } V_1 = 0, \qquad R_{21} = \frac{V_2}{I_1} = R_{rm} \text{ (A3)}$$

Matrix R can be converted to the modal (common-differential) from  $(R_m)$  by the following transformation:

$$R_m = (T_v)^{-1} \cdot R \cdot T_i = \begin{bmatrix} 0.5(R_{11} + R_{21}) & 0\\ 0 & 2(R_{11} - R_{21}) \end{bmatrix}$$
 (A4)  
Where,  $T_v = \begin{bmatrix} 1 & -0.5\\ 1 & 0.5 \end{bmatrix}$ ;  $T_i = \begin{bmatrix} 0.5 & -1\\ 0.5 & 1 \end{bmatrix}$ 

For the differential mode, according to (A4):  $R_{dd} = 2(R_{11} - R_{21}) = 2(R_t + R_r)$  (A5)

The upper and lower portions of the stripline are in parallel. As Fig.A-2(a) shown, (A5) is expanded as:

$$\begin{split} R_{dd} &= 2[(R_{t1} + R_{r1})||(R_{t2} + R_{r2})] \\ &= 2 \cdot \frac{(R_{t1} + R_{r1}) \cdot (R_{t2} + R_{r2})}{R_{t1} + R_{r1} + R_{t2} + R_{r2}} \ \ (\text{A6}) \end{split}$$
 For the differential mode, the left and right portions are in

series:

 $R_{t1,dd} = 2R_{t1}$ ;  $R_{r1,dd} = 2R_{r1}$ ;  $R_{t1,dd} = 2R_{t1}$ ;  $R_{t1,dd} = 2R_{t1}$  (A7) Thus, expression (A6) is converted to the same form as (10):

$$R_{dd} = 2 \cdot \frac{0.5(R_{t1,dd} + R_{r1,dd}) \cdot 0.5(R_{t2,dd} + R_{t2,dd})}{0.5(R_{t1} + R_{r1} + R_{t2} + R_{r2})}$$

$$= \frac{(R_{t1,dd} + R_{r1,dd}) \cdot (R_{t2,dd} + R_{t2,dd})}{R_{t1,dd} + R_{r1,dd} + R_{t2,dd} + R_{t2,dd}}$$
(A8)

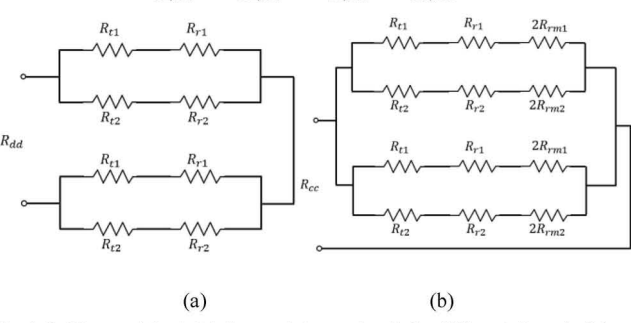


Fig. A-2. The equivlent stripline resistance circuit for differentail mode (a) and common mode (b)

$$R_{cc} = \frac{1}{2}(R_{11} + R_{21}) = \frac{1}{2}(R_t + R_r + 2R_{rm})$$
 (A9)

The upper portion and lower portion are in parallel. As Fig.A-2(b) shown, (A9) is expanded as:

$$R_{cc} = \frac{1}{2} [(R_{t1} + R_{r1} + 2R_{rm1}) | | (R_{t2} + R_{r2} + 2R_{rm2})]$$

$$= \frac{1}{2} \cdot \frac{(R_{t1} + R_{r1} + 2R_{rm1}) \cdot (R_{t2} + R_{r2} + 2R_{rm2})}{R_{t1} + R_{r1} + 2R_{rm1} + R_{t2} + R_{r2} + 2R_{rm2}}$$
(A10)

For the common mode, the left and right portions are in parallel:

$$R_{t1,cc} = 0.5R_{t1}; R_{r1,cc} = 0.5(R_{r1} + 2R_{rm1})$$

$$R_{t2,cc} = 0.5R_{t1}; R_{r2,cc} = 0.5(R_{r2} + 2R_{rm2})$$
(A11)

Expression (A10) is therefore results in the same form as (10):

$$R_{cc} = \frac{1}{2} \cdot \frac{\left(2R_{t1,cc} + 2R_{r1,cc}\right) \cdot \left(2R_{t2,cc} + 2R_{t2,cc}\right)}{\left(2R_{t1,cc} + 2R_{r1,cc} + 2R_{t2,cc} + 2R_{t2,cc}\right)}$$

$$= \frac{\left(R_{t1,cc} + R_{r1,cc}\right) \cdot \left(R_{t2,cc} + R_{t2,cc}\right)}{R_{t1,cc} + R_{r1,cc} + R_{t2,cc} + R_{t2,cc}}$$
(A12)

Thus, (10) is derived by combining (A8) and (A12).

#### ACKNOWLEDGMENT

This paper is based upon work supported partially by the National Science Foundation under Grant No. IIP-1916535.

#### REFERENCES

- X. Guo, H. Gao, G. Shen, Q. Liu, V. Khilkevich, J. Drewniak, S. De, [1] S. Hinaga, D. Yanagawa, "Design methodology for behavioral surface roughness model", in Proc. IEEE Int. Symp. EMC, Ottawa, 2016, pp. 927-931
- S. Yong, V. Khilkevich, Y. Liu, H. Gao, S. Hinaga, S. De, D. Yanagawa, J. Drewniak, "Dielectric Loss Tangent Extraction Using Modal Measurements and 2-D Cross-Sectional Analysis for Multilayer PCBs," in IEEE Trans. Electromagn. Compat., Early Access
- [3] S. Yong, Y. Liu, H. Gao, B. Chen, S. De, S. Hinaga, D. Yanagawa, J. Drewniak, V. Khilkevich, "Dielectric Dissipation Factor (DF) Extraction Based on Differential Measurements and 2-D Cross-sectional Analysis", in Proc. IEEE Int. Symp. EMC, Long Beach, CA, USA, 30 Jul-3, 2018, pp. 217-222.
- E. Hammerstad and O. Jensen, "Accurate Models for Microstrip Computer-Aided Design," in IEEE MTT-S Intl. Microwave Symposium Digest, Washington, DC, 1980.
- S. Hall, S. G. Pytel, P. G. Huray, D. Hua, A. Moonshiram, G. A. Brist, and E. Sijercic "Multigigahertz Causal Transmission Line Modeling Methodology Using a 3-D Hemispherical Surface Roughness Approach", IEEE Trans. Microw. Theory Tech., vol. 55, no. 12, Dec. 2007, pp. 2614 – 2624
- M. B. Griesi, 'Characterization of Electrodeposited Copper Foil Surface Roughness for Accurate Conductor Power Loss Modeling', Scholar Commons (Master's thesis, 2014). Retrieved from: http://scholarcommons.sc.edu/etd/2958
- P. G. Huray, O. Oluwafemi, J. Loyer, E. Bogatin, X. Ye, "Impact of Copper Surface Texture on Loss: A Model that Works", DesignCon
- [8] Y. Chu, "Method for modeling conductor surface roughness", US Patent#8527246.
- Y. Shlepnev, "Unified approach to interconnect conductor surface roughness modelling", in 2017 IEEE 26st Conference on Electrical Performance of Electronic Packaging and Systems (EPEPS2017), San Jose, CA
- [10] G. Brist, "Design Optimization of Single-Ended and Differential Impedance PCB Transmission Lines". Retrieved https://www.jlab.org/eng/eecad/pdf/053designop.pdf
- [11] Advanced Circuits Inc., 'How to Build a Printed Circuit Board', Retrieved from:

https://www.4pcb.com/media/presentation-how-to-build-pcb.pdf

- [12] M. Y. Koledintseva, T. Vincent, A. C. Scogna, S. Hinaga, "Method of Effective Roughness Dielectric in a PCB: Measurement and Full-Wave Simulation Verification", IEEE Trans. Electromagn. Compat., vol.57, no.4, Aug. 2015. pp.807-814
- [13] A. V. Rakov, S. De, M. Y. Koledintseva, S. Hinaga, J. L. Drewniak, R. J. Stanley, "Quantification of Conductor Surface Roughness Profiles in Printed Circuit Boards", IEEE Trans. Electromagn. Compat., vol.57, no.2, April. 2015. pp.264-273
- S. Hall and H. Heck, "Advanced Signal Integrity for High-Speed Digital Designs", Wiley-IEEE press, 2009.
- [15] ANSYS, Inc., ANSYS Electronics Desktop Online Help 2D Extractor (2018 release), Canonsburg, PA, USA, 2018
- CST Studio Suite 2018 Web Help. Retrieved from: www.cst.com [16]
- D. M. Pozar, Microwave Engineering, 4th ed. Wiley, Hoboken, NJ,